Model for vacancy-loop nucleation in displacement cascades

V. G. Kapinos* and D. J. Bacon

Department of Materials Science and Engineering, The University of Liverpool, P.O. Box 147, Liverpool, L69 3BX, United Kingdom
(Received 27 December 1994)

A model is proposed for the nucleation of collapsed vacancy clusters in irradiated metals, based on the principle that a vacancy loop may be nucleated in a cascade which has melted and recrystallized. The equation of thermal conduction is solved using the discretization method and initial temperature and vacancy distributions given by the MARLOWE code. The model simulates the processes of heat propagation, local melting, absorption and release of latent heat, and the redistribution of the density within the melt. Under the influence of the temperature gradient, the concentration of vacancies in the depleted zone increases. Simulation of hundreds of cascades gives the distribution of zones as a function of vacancy concentration and number of vacancies in them, and it is assumed that critical values C^{cr} and N_v^{cr} have to be achieved to produce a visible vacancy loop. However, if the concentration exceeds a value C_v^{am} under sufficiently fast cooling, for example under strong electron-phonon coupling (EPC), the melted zone cannot crystallize completely and solidifies instead to a semiamorphous core. This prevents collapse to a vacancy loop. The model has been used to calculate the yield and mean size of vacancy loops in ion-irradiated Cu, Ni, and Cu-Ge and Cu-Ni alloys. Physically reasonable values of C^{cr}, N^{cr}, and C_v^{am} have been obtained to give good agreement with experimental values of yield and size. Furthermore, the trends with alloy content can be explained, and it is found that EPC can have a strong influence on loop yield.

I. INTRODUCTION

The defects that survive intracascade recombination in irradiated materials provide a source for the evolution of radiation-induced microstructure and property changes. The vacancy component is the concern of this paper. Heavy-ion irradiations followed by transmission electron microscopy (TEM) of thin foils show that displacement cascades can collapse to form vacancy dislocation loops, but the yield and size of the loops depend on the irradiation and material parameters,[1] and the collapse process is not understood. The model introduced in this paper is based on the concepts of the "thermal spike" and "depleted zone" proposed by Seitz and Koehler[2] and Seeger.[3] These ideas have been supported by numerous computer simulation studies in recent years (see, for example, the reviews in Refs. 4–6). It has been demonstrated that the formation of depleted zones in high-energy cascades depends on the development of the thermal spike, and the mechanisms of the thermal spike influence the collapse of the depleted zone to a vacancy loop.[4,5,7–12]

Robertson, Tappin, and Kirk[7] and Tappin, Robertson, and Kirk[8] have tried to find the correlations in a wide variety of pure metals and alloys between the experimental defect yield, i.e., the fraction of cascades that produce visible vacancy loops, and material properties, including the melting temperature and the electron-phonon coupling (EPC). They have suggested that the lifetime of the thermal spike is the main parameter controlling the probability of vacancy-loop nucleation, and it depends on the melting temperature, the degree of EPC, and the solute effects (through disruption of focusons). Unfortunately, these correlations are not based on a mechanistic cascade model and cannot provide a physical explanation of ex-perimentally observed trends in the yield behavior.

Morishita et al.[9] have used the MARLOWE binary collision code (see below) to calculate the local vacancy density at the end of the cascade ballistic stage in several metals. This density was then compared with the defect yield from experiment to find a critical value of vacancy density for cascade collapse to a vacancy cluster visible by TEM. It was found that there is a correlation between the calculated critical density and the mobility of vacancies in the cascade cooling phase, but the values of the critical density found in this way do not reflect the situation in the depleted zone of a real cascade because the model does not include the redistribution of vacancies during the development of the thermal stage.

Alurralde, Caro, and Victoria[10] have proposed a hybrid model of a cascade in which the time evolution of the thermal spike was included and treated by solving a simplified version of the heat equation. The process of cascade core melting was considered and the real geometry of the melted regions was simulated by using the MARLOWE code. That model is also useful for consideration of subcascade formation in metals across a large range of primary knock atom energy. We consider that the key feature in the next stage of development of such a model is the inclusion of the process of density redistribution of the melt during the cooling of the thermal spike.

It is established that the core of a displacement cascade passes through a vacancy-rich, liquidlike phase, while the thermal spike develops.[4,5] We have shown by molecular dynamics[11] (MD) that during crystallization of this melted core, vacancies are swept to the center by the advance of the solid/liquid interface. As a result a zone where the average concentration of vacancies is several times larger

than that before the onset of the thermal spike phase is formed. A model for this effect was proposed in Ref. 11 based on the finding that the vacancy-sweeping mechanism is a consequence of the formation of compressed liquid layers at the solid/liquid interface under the influence of a large temperature gradient. The period of cascade quenching is of the order of a picosecond, however, and can be comparable with the time for the full melting transition after the ballistic phase. The formation of real liquid structure may therefore be questionable in the metals in which the lifetime of the spike is shortened by, for example, strong electron-phonon coupling (EPC). We have investigated the mechanisms leading to the final atomic structure under the influence of strong EPC,[12] and have used them in the present work to develop a model of vacancy-loop formation. The model has been employed to describe experimental results on vacancy-loop production in irradiated Ni and Cu, and Cu-Ge and Ni-Cu alloys.

II. HEAT TRANSFER SIMULATION

Consider a medium of ions which conducts heat with an isotropic thermal conductivity k. Assume heat may be generated internally—for example, by transformations involving latent heat—and lost by some kind of ionic damping system—for example, through coupling between the phonons and conduction electrons. The partial differential equation of heat conduction is then

$$\frac{\partial T}{\partial t} = \nabla\{(k/C_p\rho)\nabla T\} - \alpha_e T_e(T - T_e) + H , \qquad (1)$$

where T is the ion temperature, C_p is specific heat, ρ is the density, α_e is the constant for the cooling of the lattice by, in this case, electrons,[13,14] T_e is the electron temperature, and H is the internal heat generator function, which describes the changes of the ion temperature during the phase transformations.

Using the discretization method for a cubic array of grid points $\Delta x = \Delta y = \Delta z = a$, where a is the lattice parameter, Eq. (1) is replaced by

$$T(x,y,z,t+\Delta t) = F_0\{T(x+a,y,z,t) - T(x-a,y,z,t) + T(x,y+a,z,t) - T(x,y-a,z,t)$$

$$+ T(x,y,z+a,t) - T(x,y,z-a,t) - (6-1/F_0)T(x,y,z,t)\}$$

$$+ \Delta t \alpha_e T_e(x,y,z,t)[T(x,y,z,t) - T_e(x,y,z,t)] + \Delta t H(x,y,z,t) , \qquad (2)$$

where the Fourier number $F_0 = k\Delta t/\rho C_p a^2$ and Δt is the time step. This expression allows the temperature at site x,y,z at time $(t+\Delta t)$ to be calculated simply in terms of its own and six neighboring site temperatures at time t, all of which are known from the previous step or, for the first step, from the initial conditions.

During the phase transformation of solid to liquid, latent heat is absorbed and the change of the temperature of ions in the ith cell with coordinates $\mathbf{r}_i(x,y,z)$ is taken into account by the internal heat generator function:

$$H(\mathbf{r}_i,t) = -\delta(t - n_m^i \Delta t)\delta(\mathbf{r}_i - \mathbf{r})(L/3k_B) , \qquad (3)$$

where $\delta(x)$ is the δ function, k_B is Boltzmann's constant, L is the latent heat, and n_m^i is the time step when the conditions of the melting are achieved for this cell. When during the cooling of the thermal spike the temperature of the cell becomes less than the thermodynamical melting temperature T_m, the latent heat L is released. The way to include this amount of heat in the calculation is as follows. During the simulation of the temperature distribution, whenever a node temperature falls below T_m, the temperature is changed to T_m and the difference between the predicted temperature and T_m duly noted. During subsequent iterations this adjustment procedure continues until the cumulative total of the adjustments is equal to the value $L/3k_B$.

III. ELECTRON-PHONON COUPLING

According to Finnis, Agnew, and Foreman[14] the parameter α_e, which reflects the strength of the electron-phonon coupling, can be estimated by the formula

$$\alpha_e = \left[\frac{3\Theta_D \gamma_e v_f}{\pi^2 r_0 C_p \rho T_0}\right] , \qquad (4)$$

where Θ_D is the Debye temperature, γ_e is the coefficient of the electron heat capacity per unit volume, v_f is the Fermi velocity, r_0 is the radius of the Wigner-Seitz cell, and ρ is the density. T_0 is given by

$$T_0 = \lambda \frac{T}{r_0} \quad (T > \Theta_D) , \qquad (5)$$

where λ is the electron mean free path and T is the local ionic temperature. To estimate the value of λ the following expression can be used:[7,15]

$$\lambda = \frac{92.4(r_0/a_0)^2}{\sigma} , \qquad (6)$$

where a_0 is the Bohr radius and σ is the electrical resistivity. Flynn and Averback[13] introduced the concept of the "critical temperature" T_c above which an equilibrium can be achieved between the electron and phonon systems in a cascade region of size more than some critical radius r_c. For a spherical thermal spike with total energy Q, the value of T_c is estimated by the formula[13]

$$T_c = \frac{9T_0^6}{\Theta_D^3}\left[\frac{Q}{k_B}\right]^2 . \qquad (7)$$

The values of T_c, r_c, ρ, λ, Θ_D, and γ_e of the metals and alloys for which there are experimental data on loop nucleation are presented in Ref. 7. These data were used here for estimation of the values of α_e employed in Eqs. (1) and (2).

To calculate the spatial temperature distribution of the electron within a melted region, we assume that it is reasonable to use the diffusion approximation. Diffusion in the electronic system is much faster than in the ionic one, so a steady-state equation for the temperature distribution of the electrons, $T_e(r,t)$, can be used:[14]

$$\left[\frac{3\Theta_D v_f}{\pi^2 r_0 T_0} \right] (\langle T \rangle - T_e) + \frac{v_f r_0 T_0}{3 \langle T \rangle} \nabla^2 T_e = 0 , \qquad (8)$$

where $\langle T \rangle$ is the average ion temperature in the melted region. Within a cascade at a particular time, several regions, which we call "subzones," may be molten. We assume each to be spherical, with a radius R related to the true volume of that subzone by $R = a(3M/4\pi)^{1/3}$, where M is the number of melted cells.

The boundary conditions for Eq. (8) are

$$T_e(R,t) = T_{amb} \quad \text{and} \quad \left. \frac{\partial T_e}{\partial r} \right|_{(0,t)} = 0 , \qquad (9)$$

where we assume that the electrons are at the ambient temperature of the lattice T_{amb} at $r > R$. All calculations below were done for $T_{amb} = 300$ K. According to our estimations,[12] this assumption reasonably describes the electron behavior outside the intense thermal spike of the molten subzone because in the region $R < r < R_1$, where the average ion temperature is $\langle T \rangle_2$, the mean free path of the electrons is $\lambda = r_0 T_0 / \langle T \rangle_2$. This is considerably less than the interval $(R_1 - R)$ only for large R_1, i.e., when $\langle T \rangle_2$ decreases and becomes close to T_{amb}.

In (1) we do not use the detailed spatial distribution of the electron temperature in the melted subzones because on average the size of a subzone is comparable with the electron-phonon mean free path. The condition $\lambda \gg R$ can be satisfied completely only at the beginning of a thermal spike cooling, and that period of time is very short compared to the total lifetime of the thermal spike. For this reason $T_e(x,y,z,t)$ in Eq. (2) can be replaced by the average electron temperature $\langle T_e(t) \rangle$:

$$\langle T_e(t) \rangle = \frac{3}{R^3} \int_0^R r^2 T_e(r,t) dr . \qquad (10)$$

The electron-phonon coupling parameter α_e given by expression (4) and the average electron temperature in the melted subzone $\langle T_e(t) \rangle$ are used in Eq. (2) to simulate the evolution of the ion temperature in each melted subzone. Following the arguments above, the average electron temperature is assumed equal to the ambient lattice temperature for regions of the thermal spike outside the melted subzone(s).

IV. MELTING CRITERIA

The cascade core can become molten when the average energy supplied to each atom of this zone in the ballistic phase is higher than the value $(3k_B T_m + L)$. However, when the heat is extracted rapidly from the ionic system by strong EPC, i.e., a large value of α_e, the time t_m^i for the solid-to-liquid transformation of the ith cell of this zone becomes comparable with its time to cool below T_m. This time can be estimated using the following expressions:[12]

$$t_m^i = \infty, \quad \langle T^i \rangle < (T_m + L/3k_B) ,$$

$$t_m^i = t_A - t_B \langle T^i \rangle, \quad (T_m + L/3k_B) < \langle T^i \rangle < T_C , \qquad (11)$$

$$t_m^i = \varepsilon, \quad T_C < \langle T^i \rangle ,$$

where $\langle T^i \rangle$ is the average temperature of ions in the i cell. These conditions are based on the observations of MD simulations in Ref. 12 that the time for a small region to melt is constant for high $\langle T^i \rangle$ but increases linearly with decreasing $\langle T^i \rangle$ to the point where melting is impossible. The values of t_A, t_B, T_C, and ε were calculated for Cu in Ref. 12 and are equal to 5.83×10^{-12} s, 1.64×10^{-15} s K^{-1}, 3500 K, and 10^{-13} s, respectively. It is considered that cell i transforms from solid to liquid at the time $t^i = n_m^i \Delta t$ from the beginning of the cooling only if the following conditions are satisfied:

$$n_m^i \Delta t > t_m^i = t_A - t_B \langle T^i \rangle \quad \text{or} \quad \varepsilon$$

with

$$\langle T^i \rangle = \frac{1}{n_m^i + 1} \sum_{k=0}^{n_m^i} T^k ; \qquad (12)$$

i.e., the average ionic temperature obtained from Eq. (4) over n iterations is sufficient to ensure that melting can occur at the end of that time period.

For Ni and Ni alloys, t_m was derived from a shift of the curve described by (11) along the T axis by $\Delta T = (T_m^{Ni} - T_m^{Cu}) + (L_m^{Ni} - L_m^{Cu})/3k_B$. This means that for Ni the solid-liquid transformation requires a higher level of the temperature for a given t_m or a larger t_m for a given $\langle T^i \rangle$ compared to Cu.

The melting criteria, (11) and (12), do not take into account the influence of pressure on the kinetics of melting. To consider that properly it is necessary to take into consideration the variation of the melt density. In our previous paper[12] we considered the case when the initial vacancy concentration in the melt was 2 at. %, and all parameters in (11) were obtained for this initial concentration. Calculations using the present hybrid model showed that the average concentration of vacancies in zones that melt in Cu is in the range 1–3 at. %, thereby justifying this approach.

V. THE INITIAL CONDITIONS

The initial temperature distribution was obtained by the MARLOWE code.[16] This code simulates cascade development inside a crystalline solid as a series of isolated classical binary collisions using the Moliere potential to describe the interactions. Inelastic (electronic) energy losses may be included, as may a simple model of uncorrelated Gaussian thermal displacements of the lattice atoms. Target atoms enter the cascade process if they receive a kinetic energy greater than a minimum value of the cutoff energy E_c. A binding energy can be subtracted from the initial kinetic energy of a newly displaced atom. Cascade atoms are followed collision-by-collision until their energies fall below the value E_c. The kinetic energy of all atoms that are involved in the motion and have stopped after reducing their energy to values less than E_c

are generated as output. The coordinates of the interstitials and vacancies at the end of the collisional phase of the cascade are also generated. Unfortunately, the code does not produce detailed information about the spatial redistribution of the kinetic energy of the primary knock-on atom, and so we were forced to engage an approximation for calculating the kinetic energy distribution at the end of the ballistic phase. We assumed that the position of vacancies represents the region of a cascade in which the main part of the damage energy $E_{dam} = E_{PKA} - E_{in}$ is released, where E_{PKA} is the kinetic energy of the primary knock-on atom and E_{in} is the total inelastic (electronic) energy loss. The method for realizing this assumption in our hybrid model is as follows. In the solution of Eq. (1) by the discretization method [Eq. (2)] the initial temperature of the ith cell is calculated by the expression

$$T^i(\mathbf{r}_i, 0) = \frac{1}{3k_B} \left[\frac{n_v^i \left[E_{PKA} - E_{in} - \sum_{i=1}^{N_C} E_k^i \right]}{N_v} + \sum_{j=1}^{n_c} E_k^j \right], \quad (13)$$

where N_c is the total number of cascade atoms set into motion and stopped at the ends of the cascade trajectories according to the criterion $E_k^i < E_c$, n_C is the number of such atoms located in the cell i, N_v is the total number of vacancies generated in the cascade, and n_v^i is the number of vacancies in cell i. For the simulation of a target with a thin foil geometry, we assumed that the temperature of a cell at the surface is equal to the ambient temperature T_{amb}.

To simulate the evolution of the volume of the melt in a cascade, Alurralde, Caro, and Victoria[10] adopted an alternative idea of "restoring" the kinetic-energy profile at the end of the dynamical stage by relating the spatial distribution of the kinetic energy of cascade atoms to the spatial distribution of the total-energy deposition. A multiplication factor

$$\chi = E_{PKA} / \sum_i E_k^i$$

was calculated, where the summation is over all cells, and the energy of the ith cell was increased to χE_k^i. In this way, instead of being restored along the cascade atom trajectories, the total amount of energy was deposited at the last location of the moving atoms. The value of $\sum_i E_k^i$ is between 20 and 30% of E_{PKA}, regardless of E_{PKA},[10] and this means that the kinetic energy of cells that contain the interstitial atoms has to be increased by up to 3–5 times. This increase leads to an initial cell temperature that is much higher than the melting temperature. In the method of Alurralde, Caro, and Victoria,[10] the total numbers of interstitials and vacancies N_i and N_v located within the melted zone become approximately equal, so that the total number of surviving vacancies after solidification of the melt $\Delta N_v = N_v - N_i$ is approximately zero, and it is impossible to generate vacancy clusters with sizes comparable to those observed experimentally.

VI. A MODEL OF FORMATION OF A DEPLETED ZONE FROM THE MELT

The initial temperature distribution typically gives an irregular shape of the melted region. The fine structure of the melt usually consists of a few melted subzones. The initial number of subzones $N_{sub}(0)$ at the time of the maximum size of the melt is a function of target material and energy and mass of the incident ion. [Here and in the following, we use (0) to denote this initial time for thermal evolution.] It is considered that $M_j(0)$ melted cells form the jth subzone [$j = 1$, $N_{sub}(0)$] if they produce a three-dimensional cluster in which all molten cells have at least one neighbor within a sphere of radius $r = \sqrt{3}a$. The spatial shape of the melt and, hence, the total number of subzones change during the cooling.

The mechanism of redistribution of vacancies in the depleted subzone during melting and crystallization has been proposed earlier.[11] Using MD simulation of thermal spikes, it was demonstrated that the pressure in the melt is uniform. The pressure equalization mechanism is the redistribution of atomic density within the melt in such a way that the variation in the thermal component P_T of the total pressure, which follows the temperature distribution $T(\mathbf{r}, t)$, is compensated. This mechanism results in the formation of liquid at the periphery of the melted zone where the density is greater than that in the hotter central part. A mathematical model was developed to describe this process[11] and is used here, as follows.

Consider the structure of the melt at time $t_n = n\Delta t$. The volume per atom of the ith cell in the jth subzone consists of two parts: a temperature-dependent part and the part that depends only on the concentration of vacancies C_j^i:[11]

$$\Omega_j^i = \Omega_0(1 + \beta^* T_j^i + C_j^i) \quad \text{for } i = 1, 2, \ldots, M_j, \quad (14)$$

where $\beta^* = 3\xi \langle \gamma \rangle k_B T_j^i / B\Omega_0$, Ω_0 is the volume per atom of the liquid at zero pressure at $T = 0$ K, B is the bulk modulus of the liquid, ξ is a constant ≈ 0.6, and $\langle \gamma \rangle$ is the average Grüneisen parameter, in which we ignore the dependence on Ω_j^i and T_j^i.

The total pressure in this cell consists of the pressure at $T = 0$ K plus the thermal component given by the Grüneisen formula:

$$P_j^i(T_j^i, \Omega_j^i) = P_{0,j}^i(\Omega_j^i) + \frac{3\langle \gamma \rangle k_B T_j^i}{\Omega_j^i}, \quad (15)$$

where $P_{0,j}^i(\Omega^i)$ is the "structural" component of the pressure due solely to the position of the atoms in the ith cell at $T = 0$ K. For calculation of the density distribution of the liquid in the melt we used the following system of equations:

$$P_{0,j}^i(\Omega_j^i) + \frac{3\langle \gamma \rangle k_B T_j^i}{\Omega_j^i} = P_{0,j}^1(\Omega_j^1) + \frac{3\langle \gamma \rangle k_B T_j^1}{\Omega_j^1} \quad (16)$$

for $i = 2, 3, 4, \ldots, M_j$, and

$$\Omega_j^1 + \Omega_j^2 + \cdots + \Omega_j^{M_j} = M_j \langle \Omega_j \rangle, \quad (17)$$

where $\langle \Omega_j \rangle$ is the average volume per atom in the jth subzone, which is calculated using the average temperature $\langle T_j \rangle$ and the average concentration of vacancies $\langle C_j \rangle$ in the subzone:

$$\langle \Omega_j \rangle = \Omega_0 (1 + \beta^* \langle T_j \rangle + \langle C_j \rangle) , \qquad (18)$$

i.e., it consists of a thermal part, given by $\langle T_j \rangle$, and a defect-dependent part. The system of equations (16) and (17) is based on the requirement that the total pressure in different cells of the melt be equal, with the pressure in

cell $i = 1$ [the right-hand side of Eq. (16)] being used as the reference value at any instant.

It has been shown for Cu in Ref. 11 that the function $P_0(\Omega)$ can be approximated by the linear relationship

$$P_0(\Omega) = A - B(\Omega/\Omega_0 - 1) , \qquad (19)$$

where A is a constant and B is the bulk modulus. The present model assumed that formula (19) can be applied for any melted cell, and hence the solution of the system (16) and (17) can be expressed analytically:

$$C_j^1 = \left\{ M_j \langle C_j \rangle + \sum_{i=1}^{M_j} \left[\frac{(B\beta^* - \alpha + \alpha\beta^* T^i)T^i}{B + \alpha T^i} - \frac{(B\beta^* - \alpha + \alpha\beta^* T^1)T^1}{B + \alpha T^1} \right] \right\} \bigg/ \sum_{i=1}^{M_j} \frac{B + \alpha T^1}{B + \alpha T^i} , \qquad (20a)$$

$$C_j^i = \left\{ \frac{B + \alpha T^1}{B + \alpha T^i} C_j^1 - \sum_{i=1}^{M_j} \left[\frac{(B\beta^* - \alpha + \alpha\beta^* T^i)T^i}{B + \alpha T^i} - \frac{(B\beta^* - \alpha + \alpha\beta^* T^1)T^1}{B + \alpha T^1} \right] \right\} . \qquad (20b)$$

The ability to solve Eqs. (16) and (17) in this way makes the coupling of the redistribution of density, i.e., vacancies, in the melt with the calculation of the temperature a tractable problem.

The initial average concentration of vacancies in the jth melted subzone $\langle C_j \rangle$ is calculated from the expression

$$\langle C_j(0) \rangle = \frac{N_{v,j} - N_{I,j}}{M_j a^3} \Omega_0 , \qquad (21)$$

where $N_{v,j}(0)$ and $N_{I,j}(0)$ are the number of vacancies and interstitials in the jth subzone at the time $t = t_{max}$ when the volume of the melt achieves its maximum value. At the time $t = t_{max}$ the average concentration of vacancies in the subzone is at a minimum, and it then increases for $t > t_{max}$. This time is regarded in the model as the initial one for the calculation of the density redistribution.

Consider the situation when a subzone j at the time t_n divides into, say, three subzones at the next time step $n + 1$ (zones A, B, and C in Fig. 1). For that particular geometry, the number of vacancies trapped in the solid during the cooling from t_n to t_{n+1} is calculated by the expression

$$N_{v,j}^{cr} = \frac{a^3}{\Omega_j} \sum_{i \notin A,B,C} C_j^i(t_n) , \qquad (22)$$
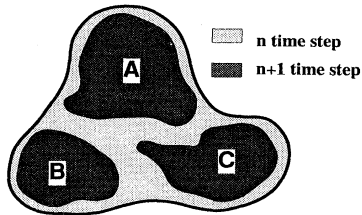
where the sum is over the cells located *outside* the melt

FIG. 1. An example of the configuration of the melt. The melt at time step n is split into three subzones A, B, and C, at the next time step.

formed at step $n + 1$. The remaining vacancies are redistributed among zones A, B, and C in accordance with the following balance equation:

$$N_{v,j}(t_{n+1}) = N_{v,j}(t_n) - N_{v,j}^{cr}(t_n)$$

$$= \frac{a^3}{\Omega_0} \left[\sum_{i \in A} C_j^i(t_n) + \sum_{i \in B} C_j^i(t_n) + \sum_{i \in C} C_j^i(t_n) \right] . \qquad (23)$$

At the beginning of cooling when the temperature gradients are high, the value of $N_{v,j}^{cr}$ can be negative, which simply reflects the fact that very compressed liquid cells exist outside the A, B, and C regions at time t_n. If $N_{v,j}^{cr} < 0$, it is considered that all vacancies are swept to the A, B, and C regions at the next time step, and this is an important mechanism for vacancy cluster nucleation in cascades. However, formally Eq. (23) does not give the correct number of vacancies in these regions because the total number of vacancies in them becomes higher than the previous value $N_{v,j}(t_n)$. This difficulty is overcome by applying a normalization factor ξ which conserves the vacancies correctly:

$$N_{v,z}(t_n) = \xi \frac{a^3}{\Omega_0} \left[\sum_{i \in Z} C_j^i(t_n) \right] \quad \text{for } Z = A, \ B, \ \text{or } C , \quad (24)$$

where

$$\xi = \begin{cases} \dfrac{N_{v,j}(t_n)}{N_{v,j}(t_n) - N_{v,j}^{cr}(t_n)}, & \text{for } N_{v,j}^{cr}(t_n) < 0 \\ 1, & \text{for } N_{v,j}^{cr}(t_n) \geq 0. \end{cases} \qquad (25)$$

VII. THE PRINCIPLE OF VACANCY-LOOP NUCLEATION IN A METAL

The principle of the model is that a vacancy loop may be nucleated in a region of a cascade, which melts and recrystallizes. The redistribution of the density within the melt under the influence of the temperature gradient leads to the "sweeping" of vacancies towards the center

of the melt, and this effect increases the concentration of vacancies in the depleted zone of the cascade after crystallization. This mechanism leads to the development of subzones, where the average concentration of vacancies $\langle C \rangle$ becomes several times larger than that produced ballistically before the onset of the thermal spike phase. The method of calculating $\langle C \rangle$ for each subzone is described in the preceding section.

A few subzones with a high concentration of vacancies $\langle C \rangle$ are usually produced within a cascade during the development of the thermal stage. The average concentration $\langle C(t) \rangle$ and the number of surviving vacancies $N_{v(t)}$ in each subzone change during the thermal spike cooling. In the computational model, the parameters $\langle C(t) \rangle$ and $N_v(t)$ are continually monitored so that for each cascade, a record is kept of the maximum value of N_v for prescribed intervals of $\langle C \rangle$, in our case 0–1 %, 1–2 %, 2–3 %, etc. In other words, all subzones of a cascade are searched at each time step to ascertain the one with the largest N_v for each interval of $\langle C \rangle$.

Two or more subzones can achieve the same level of concentration $\langle C \rangle$, for example 5 at. % at any instant, but the number of vacancies in them may be different. If this situation arises, the maximum value of N_v is selected. The record of N_v is continually updated so that if a subzone achieves a larger value of N_v for a particular $\langle C \rangle$ than that in another subzone at an earlier time, the earlier N_v value is replaced by the later one. This means that over its lifetime, each cascade is able to produce one subzone with concentration $\langle C \rangle$ and the maximum possible number of vacancies for that concentration is known. This method of accounting is restricted to the simulation of cascades with relatively low PKA energies, when the probability of subcascade formation is small. If the cascade energy is high, independent subcascades can form and that can result in the nucleation of more than one visible vacancy loop per cascade. In that case, our method has to be modified to include the criteria for multiple loop formation.

Simulation of hundreds of cascades using the MARLOWE code and the method described above gives statistics for the distribution of zones with average vacancy concentration $\langle C \rangle$ and number of vacancies N_V.

It is assumed that critical values of $\langle C \rangle = C^{cr}$ and $N_v = N_v^{cr}$ have to be achieved to produce a visible vacancy loop. The value of C^{cr} has been estimated for a simplified model of the thermal spike for Cu, Fe, and Zr in Ref. 17. For pure lattice thermal conductivity this value has to be more than 5 at. %. The critical number of vacancies N_v^{cr} consists of two parts: $N_v^{cr} = N_{v,1} + N_{v,2}$ where $N_{v,1}$ is the number of vacancies that collapse into the visible vacancy loop with radius r_{vis} (mainly a characteristic of the TEM), and $N_{v,2}$ is the number of vacancies around a loop that do not manage to join it by a diffusion mechanism. The ratio of these two values is a function of size and the average temperature of the thermal spike within the zone after crystallization. Strong electron-phonon coupling reduces this temperature and, hence, the coalescence effect because the number of diffusion jumps of the vacancies becomes fewer. The small number of vacancies in a

small zone may be another reason for a high value of $N_{v,2}$ because the strength of interaction is a function of cluster size.

In our model the defect yield for vacancy loops mimics that measured experimentally[1] and is defined as

$$Y = N/N_0 \tag{26}$$

where N_0 is a total number of computer generated cascades and N is the number of cascades in which the conditions $\langle C \rangle > C^{cr}$ and $N_v > N_v^{cr}$ are satisfied for melted zones. However, this requires modification when the electron-phonon coupling is strong, as follows.

The initial average concentration of vacancies depends on the size of the melted subzone. Strong EPC decreases the subzone maximum size and increases the initial concentration of vacancies. If the concentration of vacancies exceeds a value C^{am} during the cooling for large α_e, the melted zone cannot crystallize completely and solidifies to a semiamorphous core near the center, which prevents the collapse to a vacancy loop.[12] For consistency with experiment[1,7] the defect yield is therefore defined with N as the number of cascades in which $C^{am} > \langle C \rangle > C^{cr}$ and $N_v > N_v^{am}$ are satisfied. The selection of N_v^{am} means that small melted regions containing $N^{am} < N_v^{am}(1 + 1/C^{am})$ atoms cannot become amorphous. The assumption of a threshold value for N^{am} implies that a very small melted region (with a high value of C^{am}) undergoes spontaneous crystallization, independent of α_e, under the influence of the surrounding crystalline matrix.

VIII. RESULTS

A. The selection of inputs for the MARLOWE code

The model includes two groups of parameters that have to be defined from comparison of the calculations with the experiment. The first group defines the characteristics of a cascade at the end of the ballistic phase and is used as input in MARLOWE. The verification of these
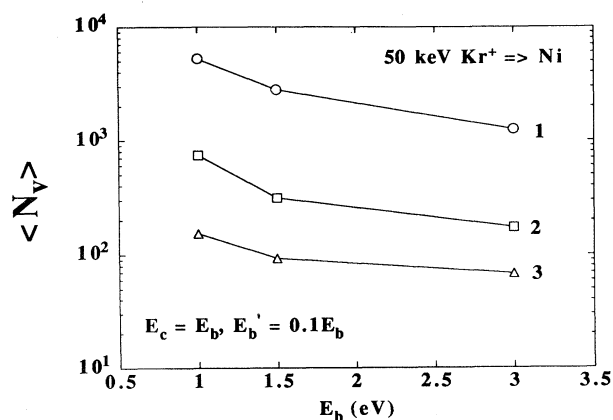
FIG. 2. Variation with the binding energy E_b of the average number of Frenkel pairs, generated at the different stages of a cascade. Curves 1 and 2 show the number of pairs at the end of the ballistic and athermal annihilation stages, respectively. Curve 3 shows the number of pairs that survive in the melt.

parameters can be done in principle by comparison with cascades simulated by molecular dynamics. The other group characterizes the conditions of vacancy-loop nucleation and includes α_e, N_v^{cr}, C^{cr}, N_v^{am}, and C^{am} and will be discussed in the next sections.

The average number of vacancies surviving the ballistic phase in MARLOWE depends on the input parameters E_c, E_b, and E_b', which are responsible for the dynamics of atoms and the separation of vacancies and interstitials. Projectiles in MARLOWE are considered as long as their kinetic energy exceeds E_c, as noted in Sec. VI. Atoms in lattice targets must overcome a binding energy E_b if they continue moving, or E_b' if they stop, but still have kinetic energy greater than E_c. We used the same relationships between these values as in Ref. 18: $E_c = E_b$ and $E_b' = \varepsilon E_b$. To demonstrate the role of these parameters in our model, we calculated the average initial number of vacancies in the melted region as a function of E_b in Ni for $\varepsilon = 0.1$ (Fig. 2). Curve 1 is the average number of vacancies produced in the cascade at the end of the ballistic stage. That number does not reflect the real number of vacancies because it includes a large number of displaced cascade atoms located near their original lattice sites. The average number of vacancies after a thermal annihilation with interstitials is shown in Fig. 2 by curve 2. The size of the spherical zone of spontaneous annihilation in this calculation was selected to be $1.3a$. There is an additional mechanism of the vacancy-interstitial annihilation at the thermal stage. The melt is the region in which interstitials completely disappear, and this decreases the average number of vacancies surviving the thermal stage. Curve 3 in Fig. 2 demonstrates the initial average number of vacancies in the melt as a function of the energy E_b. This number is sensitive to the choice of E_b, which has to be selected from the comparison of the calculated and experimental average size of the nucleated loop. In replacement events, only the target atom emerges: it must overcome only the energy $E_b' = \varepsilon E_b$, which has to be less then E_b ($\varepsilon < 1$). A value can be chosen for E_b' so that linear collision sequences resemble those in MD simulations. For example Robinson selected $\varepsilon = 0.1$ in his calculations.[18] Another possible way of selecting this parameter
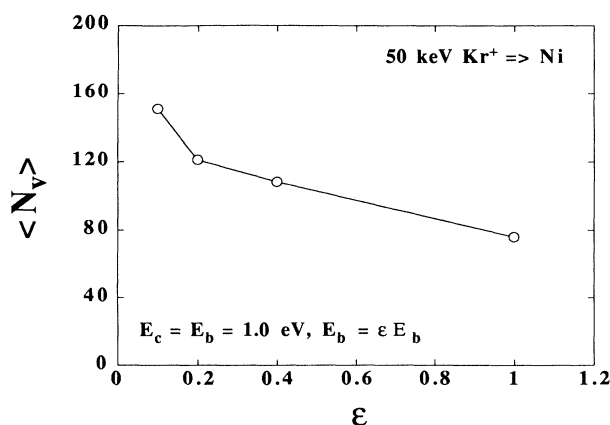
is by reasonable agreement with experiment for the size of vacancy loops. To demonstrate the importance of the parameter ε on the number of surviving vacancies we calculated the cascade efficiency (the average number of vacancies in a nucleated loop $\langle N_v \rangle$) for $E_c = E_b = 1$ eV and different values of ε (Fig. 3). It is clearly seen that an increase of ε leads to a decrease of the length of replacement sequences and, hence, to a decrease of the number of vacancies that can collapse into the loop. The mecha-

FIG. 3. The change with the parameter ε of the initial average number of vacancies surviving in the melt.
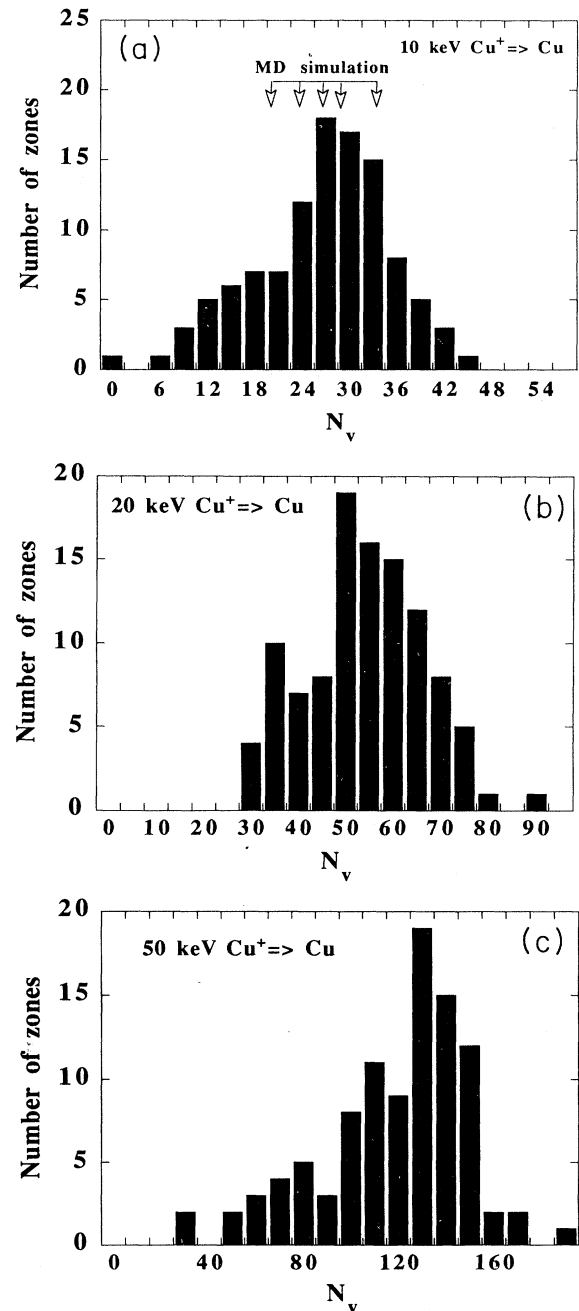

FIG. 4. Distributions of the number of vacancies surviving in melted subzones for different PKA energy: $E_{PKA} =$ (a) 10 keV, (b) 20 keV, and (c) 50 keV. The record of N_v was made at the moment when the size of the melt achieved a maximum value.
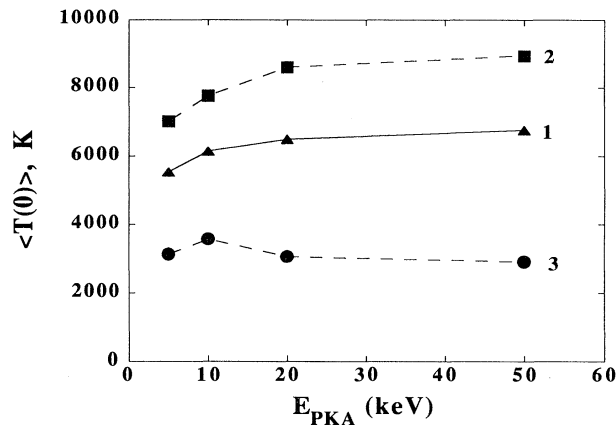
FIG. 5. The dependence of the initial average temperature in the melted subzones, $\langle T \rangle$, averaged over 100 cascades, as a function of PKA energy in Cu irradiated by Cu^+ ions at room temperature (curve 1). Curves 2 and 3 show the maximum and minimum recorded $\langle T \rangle$ among 100 cascades, respectively.

nism of this influence is the increase in the number of interstitials annihilated with the melt.

The selection of the traditional values of these parameters for Cu, for example, $E_c = 3-5$ eV,[18] cannot give results comparable with the experimental cascade efficiency. Our calculations of the distributions of vacancy loops in Cu irradiated by 30-keV Cu^+ ions demonstrate that the best agreement with experiment can be achieved with E_b selected to be 1.0 eV and $\varepsilon = 0.1$.

Robertson, Tappin, and Kirk[7] investigated several Cu-Ni alloys irradiated by 50-keV Kr^+ ions and presented the vacancy-loop size distribution in histograms. We used the average size of loops from these histograms to select reasonable values of the parameters E_c and ε for these alloys. A discussion of the problems accompanying the selection procedure of these parameters for Ni and the alloys will be given below.
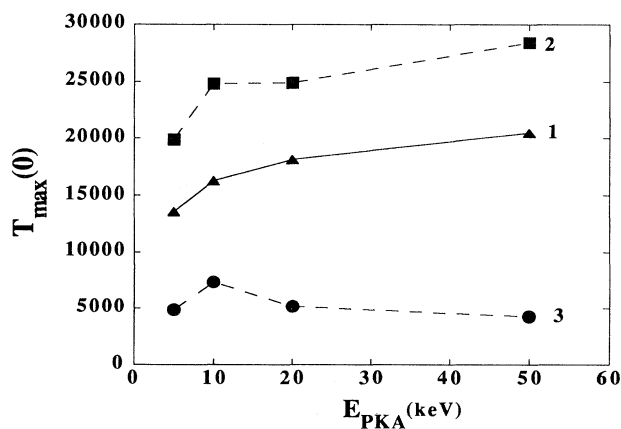

FIG. 6. The dependence of the maximum initial temperature, T_{max}, averaged over 100 cascades, as a function of PKA energy in Cu irradiated by Cu^+ ions for room temperature (curve 1). Curves 2 and 3 show the maximum and minimum T_{max} among 100 registered cascades, respectively.

B. Calculation of some cascade characteristics in Cu

The distribution in the population of molten zones as a function of the number of vacancies they contain is shown in Figs. 4(a)–4(c) for three energy values of Cu^+ ion irradiation of copper. The number of MARLOWE simulations was 100 for each energy. These distributions are plotted from the moment of time when the melt achieves a maximum size. For comparison, the results of five MD simulations of 10-keV cascades in Cu (Ref. 19) are presented in Fig. 4(a). It is seen that the hybrid model produces a number for the surviving vacancies that is comparable with MD simulations.

Figure 5 shows the average temperature in the melt at the same stage as a function of PKA energy (curve 1). Curves 2 and 3 show the maximum and minimum average temperatures that were detected during the simulation of 100 cascades at each energy in our hybrid model. The large difference between the minimum and maximum values of the temperature demonstrates that the simulation by MD of only a few cascades with high energy cannot be expected to give a representative result because there is a high probability of an "untypical" process of density redistribution in the melt for small statistics. This conclusion is supported by calculation of the maximum cell temperature in the melt, $T_{max}(0)$. The average over 100 cascades is shown as a function of E_{PKA} by curve 1 in Fig. 6. The maximum (curve 2) and minimum (curve 3) calculated values of $T_{max}(0)$ are also plotted, and they differ from each other by approximately five times. This means that there is a very strong variation of the temperature distribution in the melted zones during their generation. The temperature distribution, in turn, strongly affects the density redistribution, and for this reason the final structure of the melted and recrystallized zone may be very different for different cascades. Only simulation of a large number of cascades can provide reliable information about the average characteristics of cascades for comparison with experiment.

Figure 7 shows the change in the number of subzones per cascade $\langle N_{sub}(0) \rangle$ (solid line) and melted cells per cascade $\langle M(0) \rangle$ (dashed line) as a function of PKA energy. The data are averaged over 100 simulations. As can
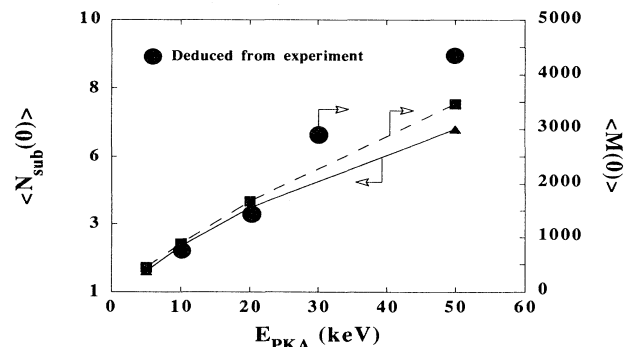

FIG. 7. The dependence of the average number of subzones per cascade and the number of melted cells per cascade on the PKA energy in Cu irradiated by Cu^+ ions at room temperature. The experimental number of melted cells in Cu_3Au, extracted from Ref. 20, are indicated.

be seen, the number of subzones at the peak of the size of the melt increases with increasing cascade energy. The increasing spatial separation of the subzones with increasing energy leads to the formation of fine structure within cascades, in which one cascade region may consist of several distinct vacancy clusters. If these clusters were to be detected as individual clusters experimentally by TEM, the defect yield could achieve a value of more than unity. It is of interest to compare the size of the melt in our model with experimental information. Jenkins and Norton[20] performed direct measurement of disordered zones in the ordered alloy Cu_3Au using TEM, and presented the measured cascade size as a function of ion energy (Fig. 3 in Ref. 20). If it is assumed that the size of the disordered zone is defined by the size of the melted region, as has been demonstrated to be reasonable by MD simulations,[21,22] the number of melted cells in Cu_3Au can be calculated using the experimentally measured size of disordered zones. The results of these calculations are shown in Fig. 7 by black circles. It is clear that the experimental and calculated results are close to each other, and this agreement may be taken as one more demonstration of the validity of the hybrid model developed here.
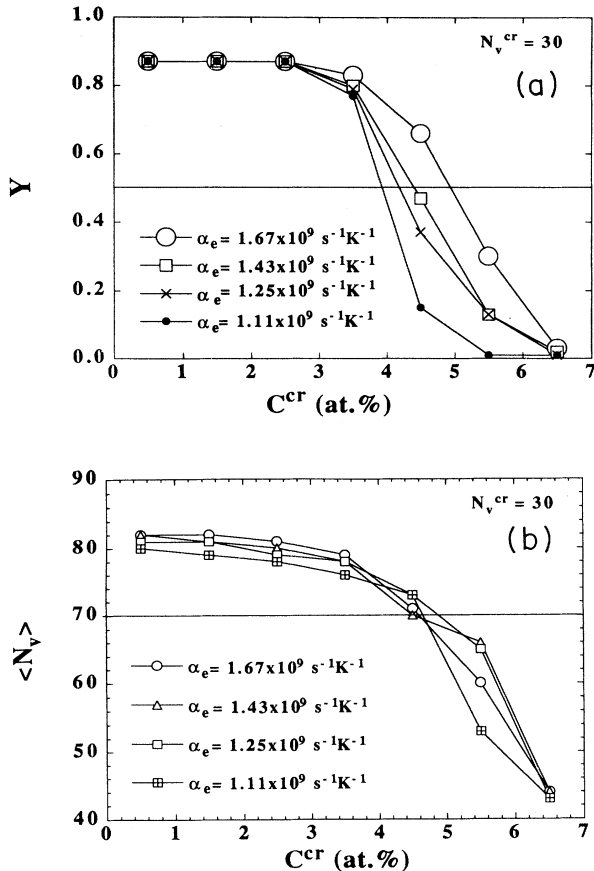
C. Cu and Cu_3Au irradiated by Cu^+ or Kr^+

The dependencies of the loop yield and $\langle N_v \rangle$ on C^{cr} in copper irradiated with 30-keV Cu^+ ions are shown in Figs. 8(a) and 8(b) for different values of the EPC parameter α_e. The curves were calculated for $N_v^{cr} = 30$. The experimental values of $Y = 0.5$ and $\langle N_v \rangle = 70$ for pure copper[23] are marked on the figures by the horizontal lines. The yield and $\langle N_v \rangle$ decrease with increasing C^{cr} for C_{cr} greater than about 3 at. %. Agreement between the theoretical and experimental values of Y can be achieved for different combinations of α_e and N_v^{cr}. For example, for the choice $N_v^{cr} = 30$ used in Fig. 8 and α_e in the range $(1.1-1.7) \times 10^9 \ s^{-1} K^{-1}$ [that range is estimated from Eq. (4) for copper parameters] the value of C^{cr} lays in the interval 4–5 at. %. For this interval the theoretical and experimental values of $\langle N_v \rangle$ are also close to each other. If other values of N_v^{cr} are selected, for example, more than 30, the values of C^{cr} are shifted to a slightly lower range. For instance, if N_v^{cr} is selected
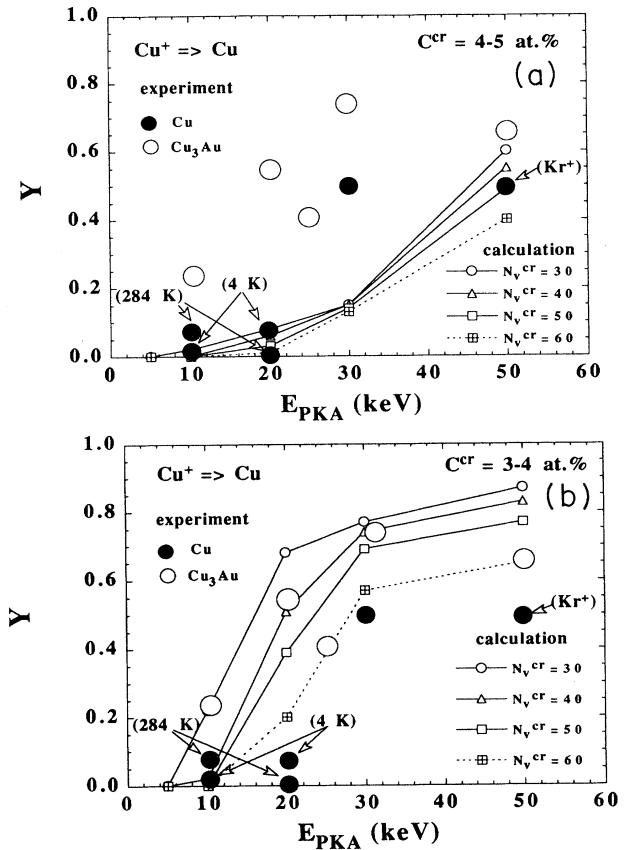

FIG. 9. Vacancy-loop yield as a function of the PKA energy. Each curve has been calculated for different values of N_v^{cr}. The black circles are the experimental data for yield in Cu at 284 K (Refs. 7 and 23). The experimental value (Ref. 27) for 10- and 20-keV irradiation of copper at 4 K is also shown. For 50-keV energy the experimental value has been obtained for Kr^+-ion irradiation. The large white circles are the experimental data for yield in Cu_3Au (Ref. 20). The calculations have been performed for the critical concentration C_v^{cr} equal to either (a) 4–5 at. % or (b) 3–4 at. %.

FIG. 8. Vacancy-loop yield (a) and average number of vacancies in a loop (b) as a function of the critical concentration of vacancies, C^{cr}. The curves have been calculated for different values of the parameter α_e as indicated. The value of $N_v^{cr} = 30$.

to be 60, the interval of C^{cr} is 3–4 at. % for the same range of α_e.

According to Eq. (4) the value of α_e^{Cu} has to be $\approx 10^9$ $s^{-1} K^{-1}$, and the theoretical dependencies of the loop yield on the primary-knock energy E_{PKA} in Cu for this value of α_e are presented in Figs. 9(a) and 9(b) for different magnitudes of C^{cr} and N_v^{cr}. The experimental results obtained for pure Cu are also plotted on these figures. Furthermore, it is reasonable to assume that the character of radiation damage of Cu$_3$Au alloy is similar to pure copper, and so we have compared our calculations with the experimental data for this material also. It is important to note that the method for estimating the yield in Cu$_3$Au is different from that for pure Cu. In the alloy, vacancy loop yield was defined as the ratio of the number of visible dislocation loops to the number of visible black dots, i.e., disordered zones, observed in super-lattice reflections,[20] a method that represents the probability of cascade collapse much more precisely than that based on the estimated ion dose.

For Cu and Cu$_3$Au the experimentally observed yield increases with increasing E_{PKA} and saturates at the level 0.6–0.7 for ions having energy more than 50 keV. Comparison of the calculations with experiment demonstrates that the theoretical curves for any N_v^{cr} cannot describe the experimental behavior even qualitatively for C^{cr} selected from the interval 4–5 at. % [Fig. 9(a)]. Reasonable agreement between the predicted and experimental yield can be achieved only for $C_{cr} = 3$–4 at. % and $N_v^{cr} = 50$–60 [Fig. 9(b)].

The rise and saturation of the yield with the increase of E_{PKA} is explained in the model as the result of the beginning of subcascade formation for E_{PKA} greater than about 30 keV. At this energy, some zones may split into subzones having $\langle C \rangle > C^{cr}$, but some of these have a size less than N_v^{cr} and, as a result, do not produce visible vacancy loops.

The dependence on E_{PKA} of the average number of vacancies in loops $\langle N_v \rangle$ extracted from experiment and our calculations is shown in Fig. 10. The theoretical results
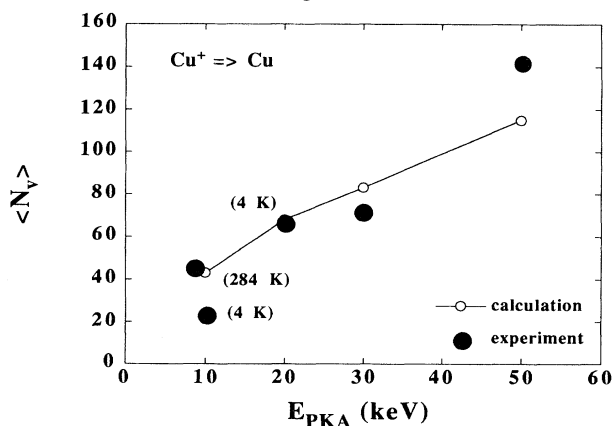
are for the critical parameters found above, i.e., $C^{cr} = 3$–4 at. % and $N_v^{cr} = 50$–60. It is seen that the discrepancy in the predicted average number of vacancies in the loops for $E_{PKA} = 50$ keV is $\approx 20\%$. Although this difference is not large, a possible explanation is that some loops coalesce during the experimental irradiation due to their mutual interaction. This would decrease Y and lead to the formation of a small population of large loops in the experimental distributions.[7,23] For example, the population of loops in Cu irradiated by 50-keV Kr$^+$ consists of $\approx 10\%$ with a size of more than 5–6 nm. The number of vacancies in such loops is more than 350–400, and it is impossible to generate such large sizes in the bulk of Cu using the MARLOWE code in the scope of our hybrid model. We also note that our model predicts a yield of 0.6–0.7, which is higher than the experimental value of 0.5 for pure Cu, but still comparable with the yield 0.6 in the alloy Cu$_3$Au for $N_v^{cr} = 60$. Unfortunately there is no information about the size of the loops in Cu$_3$Au, but it is clear that each loop is connected precisely with a spatially isolated cascade region formed in the bulk of the sample. That may be the reason why the yield in the alloy is a little higher than in pure Cu because only loops that did not spatially overlap and interact with the surface were taken into consideration.

D. Cu-Ge alloy irradiated by 30-keV Cu$^+$

Consider now the Cu-Ge alloy system. The defect yields and mean loop image diameters for several Cu-Ge alloys irradiated by 30-keV Cu$^+$ ions were measured by Stathopoulos et al.[23] The defect yield increases as the content of Ge in solution increases, with a maximum yield of 0.74 registered for the Cu-7.6 Ge at. % alloy. The relative change in the yield is 0.24 between Cu and Cu-7.6 at. % Ge, but the melting temperature difference is only 100 K, and this would seem to be too small to have any significant effect on the nucleation of a vacancy cluster in the cascade core. It is therefore reasonable to investigate whether the EPC may be responsible for the
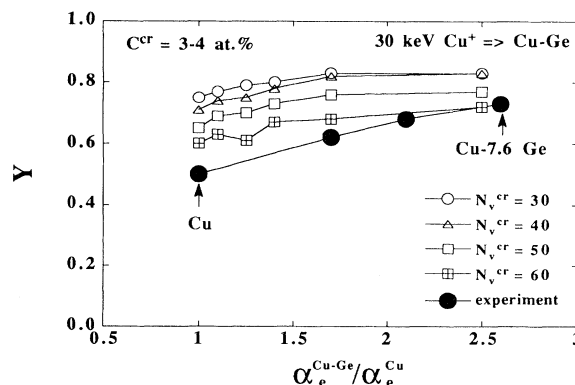
FIG. 10. The dependence of the average number of vacancies in loops on the PKA energy in Cu irradiated by Cu$^+$ ions at room temperature. The experimental value (Ref. 27) for 10 and 20 keV for irradiation at 4 K is also shown. For 50-keV energy the experimental value is for Kr$^+$-ion irradiation.

FIG. 11. Vacancy-loop yield as a function of the EPC strength parameter α_e. The model curves were evaluated for values of the critical number of vacancies N_v^{cr} shown. The calculations were performed for the critical concentration, $C_v^{cr} = 3$–4 at. %. The black circles are the experimental data (Ref. 23) for yield in Cu and Cu-Ge alloys.
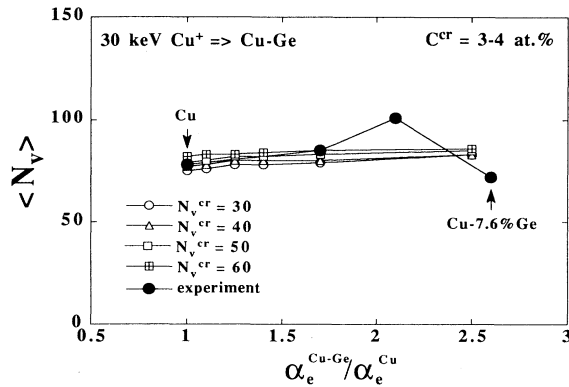
FIG. 12. Average number of vacancies in zones in Cu as a function of the EPC strength parameter α_e. The curves were calculated for values of the critical number of vacancies N_v^{cr} shown. The critical concentration C_v^{cr} was taken as 3–4 at. %. The black circles are the experimental data (Ref. 23) for yield in Cu and Cu-Ge alloys.

variation in the loop yield of this alloy. Since the difference between the atomic mass of Cu and Ge is small, the alloy in our model is considered simply as pure Cu having different values of α_e for the different Ge content. In the preceding section the values $C^{cr}=3$–4 at. % and $\alpha_e^{Cu}=1\times10^9$ s^{-1} K^{-1} were selected to describe the dependence of the yield in Cu on the energy of the incident ions. The ratio of $\alpha_e^{Cu\text{-}Ge}/\alpha_e^{Cu}$ for Cu-Ge alloys can be estimated from Eqs. (4) and (7) by the formula

$$\frac{\alpha_e^{alloy}}{\alpha_e^{Cu}}=\frac{(\Theta_D^{alloy})^{1/3}\gamma_e^{alloy}(T_c^{Cu})^{1/3}C_p^{Cu}}{(\Theta_D^{Cu})^{1/3}\gamma_e^{Cu}(T_c^{alloy})^{1/3}C_p^{alloy}} . \quad (27)$$

The values of T_c, γ_e, and Θ_D as functions of Ge concentration in the range 0–10 at. % can be taken from Table 5 in Ref. 7. It is found that the ratio $\alpha_e^{alloy}/\alpha_e^{Cu}$ increases from 1 to 2.5 as the Ge content increases from 0 to 8 at. %.

The experimental and calculated yields for these alloys for $N_v^{cr}\geq30$ are shown in Fig. 11, from where it is seen that good agreement between predicted and experimental yield is achieved for $N_v^{cr}\geq60$. There is also good agreement between the experimental and calculated average numbers of vacancies in loops if the same N_v^{cr} and α_e values are selected, as shown by the data in Fig. 12. The results obtained by the model do not fit the increase in

the experimental average size of loops in the Cu-3.9 Ge at. % alloy, but this may be due to the experimental problem of accurately measuring the image size of the small loops with a vacancy number near N_v^{cr}.

The growth of the yield of Cu-Ge alloys with increasing Ge content is interpreted in the model developed here as resulting from the increase of the EPC strength. The EPC strength for the Cu-7.6 at. % Ge alloy is only 2.5 times higher than that of pure Cu, but even that difference has the effect of producing a considerable increase in the yield. The average number of vacancies in the loops is not as sensitive to the EPC strength as the yield according to our model.

E. Cu-Ni alloy irradiated by 50-keV Kr$^+$

The second alloy system analyzed in the scope of the hybrid model developed here is the Cu-Ni alloy series irradiated by 50-keV Kr$^+$ ions to a dose of 2×10^{11} ions cm^{-2}. The values of yield and average image diameters measured experimentally for Cu-Ni alloys by Robertson, Tappin, and Kirk,[7] and the ratios of the estimated values of α_e [as in Eq. (27) using data from Ref. 7] are summarized in Table I. The value of the defect yield for pure Ni was taken from Ref. 7 and, since loop counting is somewhat subjective, this value may be artificially high.[7] In comparing the calculations with experiment we shall assume that the yield for pure Ni and Cu-90% Ni is the same. The experimental yield increases from 0.49 for pure Cu to 0.6 for the alloy with 20 at. % Ni, a trend that is similar to that found for the Cu-Ge system, but the yield then decreases rapidly to a low value at the Ni-rich end of the composition range. An interpretation of this behavior is proposed in this section.

The addition of Ni to Cu has a strong effect on the strength of the electron-phonon coupling (Table I). For the Ni content from 40 to 90 % the value of $\alpha_e^{alloy}/\alpha_e^{Cu}>3$. Based on the approach used for Cu-Ge alloys in the preceding section, the result of the influence of a low value of α_e on the yield and $\langle N_v\rangle$ can be easily predicted from Figs. 11 and 12. To do that, all curves should be extrapolated into the range of $\alpha_e^{Cu\text{-}Ge}/\alpha_e^{Cu}>3$, where there is a tendency for the yield curves to be constant at the level 0.8–0.9. These curves are for 30-keV irradiation, but calculations for $E_{PKA}=50$ keV demonstrate a similar trend in the calculated yield behavior for the high α_e. Thus, it is seen that the use of the present

TABLE I. Experimental values of the defect yield and the mean image diameters for Cu-Ni alloys taken from Ref. 2. The average number of vacancies in the loops and the theoretical estimate of the ratios of the parameters α_e are also given.

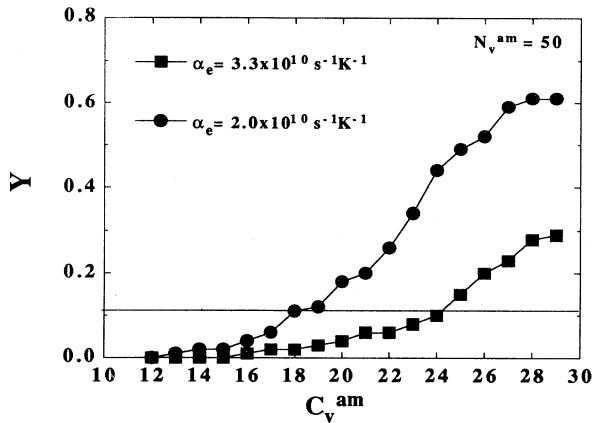| Material (at. %)	Defect yield	Mean image diameter (nm)	Mean number of vacancies	$\alpha_e^{Ni}/\alpha_e^{alloy}$
Cu	0.49	3.3	150	46.8
Cu-20 Ni	0.6	3.2	142	7.4
Cu-40 Ni	0.39	3.0	127	2.5
Cu-60 Ni	0.14	2.3	78	1.3
Cu-80 Ni	0.09	2.4	85	≈1.0
Cu-90 Ni	0.11	1.9	53	≈1.0
Ni	(0.33?)$\Longrightarrow$0.11	2.2	71	1.0

FIG. 13. Calculated vacancy-loop yield in Ni as a function of C_v^{am}. Calculations for different values of the EPC strength parameter α_e are as indicated. The experimental yield, $Y = 0.11$, is indicated by the horizontal line.

hybrid model for describing the yield in the Cu-Ni alloy system by simply increasing the parameter α_e predicts a constant and high yield for increasing Ni content, and thus gives results, which are not found in experiment. It therefore appears that, for strong EPC, an additional mechanism is important in the collapse process, and it should be incorporated in our model. The idea of such a mechanism has been proposed in Ref. 12 and has been discussed briefly in Sec. VII. It is based on the finding from MD simulations[12] that for large α_e, the core of a cascade containing a high concentration of vacancies ($> C^{am}$) is unlikely to recrystallize completely and will solidify to a semiamorphous, or highly defective, zone that cannot collapse to form a loop. Thus, the additional parameters C^{am} and N_v^{am} have to be considered here in order to describe the behavior of the material under the strong electron-phonon coupling appropriate to the Cu-Ni system.

To investigate the influence of C^{am} on the calculated yield the distributions of the zones were calculated for
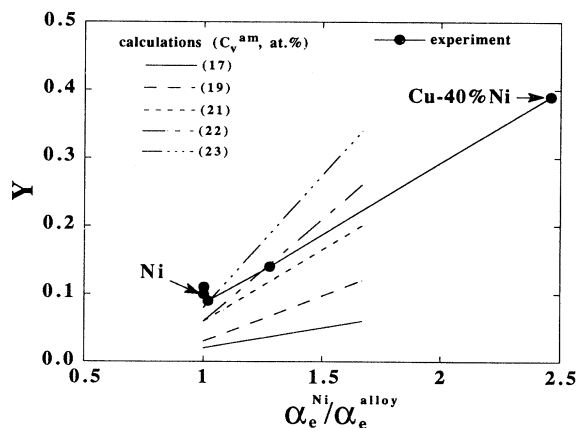

FIG. 14. Calculated and experimental vacancy loop yield as the functions of the ratio of the EPC strength parameters for Cu-Ni alloys, α^{alloy}, and pure Ni, α^{Ni}. Calculations for different values of the parameter C_v^{am} are as indicated.
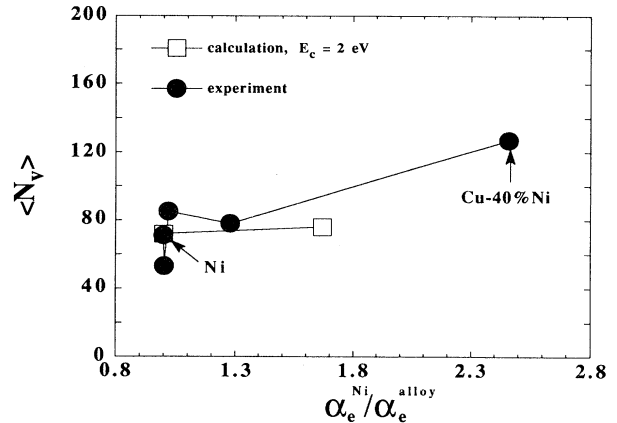

FIG. 15. Calculated and experimental average number of vacancies in loops as functions of the ratio of the EPC strength parameter for Cu-Ni alloys, α^{alloy}, and pure Ni, α^{Ni}. Calculations for different values of the parameter C_v^{am} are as indicated. The value of the MARLOWE parameter E_c was 2 eV and $\varepsilon = 0.1$.

different α_e in Ni irradiated by 50-keV Kr$^+$ ions. The calculations were performed for $\varepsilon = 0.1$ and $E_c = 2.0$ eV. The value of E_c for Ni was selected to be double that for Cu, since this reduces the value of $\langle N_v \rangle$ in Ni to half that of Cu (see Table I). The yield of zones in Ni with $\langle C \rangle < C^{am}$ and $N_v < N_v^{am}$ is shown in as a function of C^{am} in Fig. 13 for $\alpha_e = 2 \times 10^{10}$ and 3.3×10^{10} s^{-1} K^{-1}. [According to the data from Table I, α_e for Ni is $\approx (2-3) \times 10^{10}$ s^{-1} K^{-1}, if α_e for Cu is taken to be $\approx 1 \times 10^9$ s^{-1} K^{-1}]. The experimental loop yield for Ni (which, as noted above, we take to be the same as for the Cu-90 at. % Ni alloy) is shown in Fig. 13 by the horizontal line $Y = 0.11$. It is seen that this low yield can be achieved for $C^{am} > 20$ at. % for $\alpha_e = 3.3 \times 10^{10}$ s^{-1} K^{-1}. Increasing α_e decreases the yield because the fraction of zones that can achieve the average concentration of $\langle C \rangle = C^{am}$, and hence cannot collapse, is increased. In contrast to the yield, the average number of vacancies $\langle N_v \rangle$ does not depend on the values of C^{am} or α_e and is defined totally by the value of E_c. For pure Ni it is approximately 70–75 vacancies.

The calculated dependences of the yield and $\langle N_v \rangle$ on the ratio $\alpha_e^{Ni} / \alpha_e^{alloy}$ are plotted in Figs. 14 and 15. The former are shown as functions of C^{am}. Also shown in the figures are plots of the experimental yield and $\langle N_v \rangle$, which were taken from Table I. It is seen that the value and slope of the calculated yield curves increase with increasing C^{am}, and the calculated and experimental yield behavior are close to each other for $C^{am} = 21-22$ at. %. In contrast to the yield, the calculated average number of vacancies in loops is almost independent of the small variation in the $\alpha_e^{Ni} / \alpha_e^{alloy}$ ratio (Fig. 15). Unfortunately, the trend in the experimental sizes in the range of the ratio from 1.3 to 2.5 (Fig. 15) is not defined exactly, and so for this reason it is difficult to compare our calculations precisely with experiment.

The production of defects in the Cu-Ni alloy depends on the content of Ni, but if we wish to assess the yield and $\langle N_v \rangle$ for different Cu-Ni alloys using the estimated

value of C^{am} for pure Ni, it is necessary to select correctly the values of the parameters E_c and ε, which are functions of the alloy content. An increase in the number of surviving vacancies by variation of E_c will result in an increase in the size of the region in which vacancies are formed and redistributed. Because the vacancy coordinates are used to restore the initial temperature profile in our model in accordance with expression (13), the initial temperature gradient depends on the value of E_c and is decreased when E_c is decreased, because of the increase in the size of the melted region. The reduction of the temperature gradient decreases the total level of average concentration of vacancies in zones during the cooling of the thermal spike. This means that cascades calculated for the same E_{PKA} but for different E_c, would generate an identical yield only for different C^{am}. It is important to note that the sensitivity of the initial temperature profile to the choice of E_c is demonstrated only for a system with strong EPC. In the absence of an accurate dependence of E_c on the concentration of Ni and Cu-Ni alloys it has been assumed to be constant and equal to 2 eV for Ni content in the range 50–100 at. %. In this interval of concentration the variation of the ratio $\alpha_e^{Ni}/\alpha_e^{alloy}$ is small and the value of $\langle N_v \rangle$ is approximately constant. For a Ni content of 40 at. % the ratio $\alpha_e^{Ni}/\alpha_e^{alloy}$ becomes higher than 2 and the defect size increases to approximately 130. It therefore appears that the defect production in this alloy is intermediate between pure Ni and pure copper. For this alloy it is difficult to select the parameters E_c and ε is such a way to satisfy the conditions that the calculated magnitudes of yield and average defect size would be ≈ 0.4 and ≈ 130, respectively, for a constant value of $C^{am} \approx 21-22$ at. %. The use of a proper variation of E_c (or ε) in Cu-Ni alloys will be possible in our hybrid model only after additional information about the dependence of the initial temperature profile on the solute concentration is known: this is not available at the moment.

IX. DISCUSSION

In this paper we have proposed a new model for description of the thermal stage of a cascade. The MARLOWE binary-collision code was used to simulate the initial spatial distributions of point defects and kinetic energy in the cascade damage region with real geometry. Assuming that the damage energy is concentrated near the positions of vacancies, the initial kinetic energy profile was restored and used for calculation of the initial temperature distribution in the thermal conductivity equation. In the approximation of Alurralde, Caro, and Victoria[10] the damage energy is redistributed among the cascade atoms, which have ceased movement at the end of the ballistic stage. That leads to the result that approximately all interstitials are located within the melt and the total number of surviving vacancies after crystallization of the melted subzones is approximately zero. In contrast, our approach gives the physically reasonable result that each melted zone contains an excess number of surviving vacancies.

It has not proved possible so far to treat EPC rigorously in the context of MD simulations. The procedure used in Ref. 12, in which atoms are damped with a relaxation constant proportional to $1/\alpha_e$, is consistent with the approach of Ref. 14 outlined in Sec. III, but is at best a crude approximation to what is undoubtedly a complex phenomenon. For this reason, the interpretations presented here of dependencies on α_e should be considered as illustrative of trends rather than accurate descriptions of EPC phenomena.

The disadvantage of our method is the sensitivity of the size of the melt to the number of generated defects for a system with strong EPC. In the case of weak EPC the size of the melt at the maximum is almost independent of the initial spatial distribution of temperature and is defined only by the magnitude of the damage energy. For strong EPC, the phonon diffusion (which is much slower than diffusion in the electronic system) does not significantly influence the broadening of the temperature profile. The temperature behavior in this case is defined by the simplified version of Eq. (1):

$$\frac{\partial T}{\partial t} = -\tau^{-1}(T - T_e) + H , \qquad (28)$$

where τ is a relaxation time proportional to $1/\alpha_e$. The solution of (28) follows the simple relationship: $T \sim T_0 \exp(-t/\tau)$, where T_0 is the initial temperature. Thus, for strong EPC the initial size of the melt cannot increase with time and depends solely on the initial temperature distribution.

In the present work we used the simplest direct relation between the spatial distribution of vacancies and kinetic energy. In the scope of the MARLOWE code that was realized simply by the variation of the inputs E_c and ε. A simple way was used to select these parameters in which the average number of vacancies in the melt was correlated directly with the experimental average number of vacancies in loops. The parameters $E_c = 1$ and 2 eV for constant $\varepsilon = 0.1$ can reproduce the experimental average sizes of vacancy loops in pure Cu and Ni. In future work we propose to use molecular-dynamics simulations for the correct selection of these MARLOWE code inputs.

In this paper we have considered some pure metals and alloys that demonstrate different responses to the influence of electron-phonon coupling in the scope of this new theoretical model of vacancy-loop nucleation. According to this, a vacancy loop is nucleated in the region of a cascade, which, after melting and recrystallization, reaches the critical concentration of vacancies. It has been shown that in Cu irradiated by 30-keV Cu^+ ions the cascade regions collapse into vacancy loops if the average concentration of vacancies in them is more than 3–4 at. %. Choice of a critical concentration higher than 3–4 at. % cannot reproduce the experimentally observed saturation of the yield with increasing E_{PKA}. The saturation is explained by the tendency of the cascade core to split into small melted subzones, each of which has an average number of vacancies less than the critical value $N^{cr} = 60$. Only loops containing an average number of more than 60 vacancies in our model can produce a yield close to the experimental value 0.5. However, to produce a circular loop of diameter 1.5 nm, which is visible by TEM, it is

necessary to collect together only approximately 30 vacancies. To explain this difference we suppose that in reality it is difficult to expect that all vacancies could collect together to form a vacancy loop in a small depleted zone with an average concentration of 3–4 at. %. Some might be frozen at the periphery of the zone due to the lack of time for migration to the center during cooling. Additionally, the thermodynamic forces, which act on the migrating vacancies and drive them in the direction of the loop nuclei, are functions of the total number of vacancies in the depleted zone. For example, the binding energy of a vacancy with a small loop increases rapidly as the loop size increases. Thus, there is a size factor for vacancy-loop nucleation in metals, which influences the probability of collapse of a depleted zone into a loop.

Using the same MARLOWE parameters as for Cu, the Cu-Ge alloy system has been examined. The yield in this system has been found experimentally to increase with the addition of Ge. An increase in the Ge content results in an increase of the EPC, and in our model this leads to an increase in the magnitude of the yield. The physical reason behind this effect is the decrease in the size of the melt and the increase in the average temperature gradient. As a result, the number of zones with an average concentration of vacancies of more than 3–4 at. % becomes higher and that increases the value of the yield. The average size of the calculated loops is not predicted to depend on the variation of the EPC strength, however. This is in partial conflict with experiment, where from comparison of the size distribution for Cu with that obtained for Cu-3.9% Ge, it has been concluded that larger defect images are produced in this alloy,[23] but that on further increasing the Ge content to 7.6 at. % the size distribution is similar to that observed for pure copper. Analysis of other Cu alloy systems [for example Cu-Al (Ref. 23)] demonstrates the absence of any universal influence of the alloy content on the mean or peak image diameter of vacancy loops. It is known that loop counting and sizing in these systems is somewhat subjective, especially if we take into account that half or more of the depleted zones (or loops) contain too few vacancies to be visibly detected. In such conditions any small variations in the critical number of vacancies would have a strong influence on the monitoring of the size distribution.

We have not yet investigated the influence of the sample ambient temperature on Y and all calculations have been performed for $T_{amb} = 300$ K. We anticipate that the ambient temperature can influence Y through the mechanism of EPC because the average electron temperature $\langle T_e \rangle$ depends on T_{amb}. Increasing T_{amb} leads to increasing $\langle T_e \rangle$, but we believe that the sensitivity of $\langle T_e \rangle$ to T_{amb} is not large because the value of $\langle T_e \rangle$ is mainly defined by the average temperature of ions in the thermal spike. Qualitatively, an increase of T_{amb} would produce the effect of increasing the EPC and this, for the metals with small EPC, may lead to an increase in the value of the loop yield.

Our simulation of the vacancy loop nucleation process has been performed without consideration of the influence of a nearby surface on defect production under cascade condition. According to some recent MD investigations[24,25] damage production near a surface can be far different from that in the bulk. If the melted core of a cascade crosses the surface, the defect production efficiency can be increased by several times. If this were to occur in ion-beam irradiation of thin foils, it would result in a large yield and experimental distributions of image sizes that are several times higher than those expected from statistical size fluctuations for bulk irradiation. However, there is no evidence that this effect occurs to any significant extent at the ion energies considered in the present work. The formation of loops with an appropriate Burger vector results in glide towards, and loop loss, at the surface.[23] This process can be sensitive to the impurity content and, possibly, may explain the nonlinear variation in the average and peak sizes of the loop distributions in Cu-Ge alloy and other alloys.[23]

The MD simulation of vacancy-loop nucleation in pure Cu with different values of α_e has provided new insight into the influence of strong EPC on the yield of loops in metals. The low yield observed may be the result of the formation of a semiamorphous core in the resolidified region of a cascade.[12] A few factors influence the probability of the appearance of such a core. The most important is the EPC strength. In systems with strong EPC the initial temperature distribution influences the initial size and shape of the melted region. The size of the melt influences the level of the initial average temperature gradient, which in turn affects the probability of the formation of a zone with a high level of vacancy concentration. The size of the damage region depends on the irradiation and material parameters, such as ion mass, energy, impurity content, temperature, and others. These factors may influence the yield in metal systems with strong enough EPC in a way that cannot be easily predicted by using only simple correlations between material properties and irradiation conditions.[7]

The strong EPC reduces the lifetime of the molten zone, and the rapid reduction of the temperature can freeze the disordered structure of the melt. Comparison of the calculations with experiments has demonstrated that there is a critical concentration of vacancies above which the semiamorphous core should be formed. Our MD simulations for a one-dimensional model of the thermal spike[12] showed this mechanism in metals with strong EPC. Recently, the amorphization process in a cascade has been demonstrated in NiAl using the MOL-DYN code for a true three-dimensional simulation of a cascade.[26] It seems clear that in the future it will be necessary to investigate the conditions for amorphization as a function of the size of the melted region and value of α_e. In the present calculations we assumed that a small melted region containing 100 atoms cannot become amorphous but that assumption has to be proved by MD simulations. Selection of values of this parameter less than 100 slightly increase the value of C^{am} extracted from the experiment.

X. CONCLUSIONS

(1) The new hybrid model of vacancy cluster nucleation in displacement cascades proposed here consists of two parts. The first uses the MARLOWE code simula-

tion of the ballistic phase of cascade evolution to produce the initial distribution of the kinetic energy and Frenkel pairs. The second employs the continuum approximation to describe the thermal stage. This approach allows cascades to be studied under conditions beyond the capability of molecular-dynamics simulations.

(2) Electron-phonon coupling (EPC) has been included in the model in accordance with the treatment of Finnis, Agnew, and Foreman.[14]

(3) It has also been possible to include new mechanisms to describe the behavior of the heated cascade region. (a) the melting time t_m to establish the moment when a liquid structure is formed in the cascade core has been incorporated. It has been shown that the maximum size of the melted region in a metal is a function of not only the initial kinetic energy distribution but also the total time available for the solid-liquid transformation. (b) When the average concentration of the vacancies in the melt reaches some critical value C_v^{am} during the cooling, then for strong EPC a semiamorphous structure is formed which prevents the formation of a vacancy loop.

(4) The model has been employed to investigate vacancy loop nucleation in irradiated Ni and Cu, and Cu-Ge and Ni-Cu alloys. Approximately 100 cascades were simulated for each metal at each irradiation condition considered in order to generate statistically representative results, and the vacancy-loop yield and size distribu-tion have been predicted. This provides for direct comparison with TEM experimental data on these metals.

(5) From this analysis it has been established that for nucleation of vacancy loops in Cu the average vacancy concentration in the depleted zone has to achieve a level of more than 3–4 at. %. Only zones with more than 60 vacancies can produce visible vacancy loops.

(6) The observed increase of the yield in Cu-Ge alloys with increasing Ge content is explained by the increase of the EPC strength.

(7) The low yield in Ni is considered to result from the formation of depleted zones, which cannot fully crystallize but, under the influence of strong EPC, retain a partially amorphous core. This prevents the collapse of zones to loops. An increase of the content of Cu in Ni-Cu alloys increases the loop yield because the EPC strength decreases and the probability of recrystallization and loop nucleation in the disordered core becomes higher. These trends are in good agreement with experiment.

ACKNOWLEDGMENTS

*On leave from Department of Radiation Materials Science, Russian Scientific Centre "Kurchatov Institute," Moscow 123592, Russia.

[1]C. A. English and M. L. Jenkins, Mater. Sci. Forum 15-18, 1003 (1987).

[2]F. Seitz and J. S. Koehler, Solid State Phys. 2, 307 (1956).

[3]A. Seeger, Proceedings of the 2nd United Nations International Conference on Peaceful Uses of Atomic Energy, Geneva, 1958 (United Nations, New York, 1958), Vol. 6, p. 250.

[4]T. Diaz de la Rubia and M. W. Guinan, Mater. Res. Forum 97-99, 23 (1992).

[5]D. J. Bacon and T. Diaz de la Rubia, J. Nucl. Mater. 216, 275 (1994).

[6]R. S. Averback, J. Nucl. Mater. 216, 49 (1994).

[7]I. M. Roberston, D. K. Tappin, and M. A. Kirk, Philos. Mag. A 68, 843 (1993).

[8]D. K. Tappin, I. M. Roberston, and M. A. Kirk, Philos. Mag. A 70, 463 (1994).

[9]K. Morishita, H. L. Heinisch, S. Ishino, and N. Sekimura, J. Nucl. Mater. 212-215, 198 (1994).

[10]M. Alurralde, A. Caro, and M. Victoria, J. Nucl. Mater. 183, 33 (1991).

[11]V. G. Kapinos and D. J. Bacon, Philos. Mag. A 68, 1165 (1993).

[12]V. G. Kapinos and D. J. Bacon, Phys. Rev. B 50, 13 194 (1994).

[13]C. P. Flynn and R. S. Averback, Phys. Rev. B 38, 7118 (1988).

[14]M. W. Finnis, P. Agnew, and A. J. E. Foreman, Phys. Rev. B 44, 567 (1991).

[15]N. W. Ashcroft and N. D. Mermin, Solid State Physics, edited by W. B. Saunders (Academic, Philadelphia, 1976), p. 52

[16]M. T. Robinson, "MARLOWE, binary collision cascade simulation program version, 13: User's Guide," Oak Ridge National Laboratory (1992).

[17]V. G. Kapinos, Yu. N. Osetskii, and P. A. Platonov, J. Nucl. Mater. 165, 286 (1989); 170, 66 (1990); 184, 127 (1990).

[18]M. T. Robinson, Nucl. Instrum. Method B 48, 408 (1990); 67, 396 (1992).

[19]C. A. English, W. J. Pythian, and A. J. E. Foreman (private communication).

[20]M. L. Jenkins and N. G. Norton, Philos. Mag. A 40, 131 (1979).

[21]F. Gao and D. J. Bacon, Philos. Mag. A 71, 42 (1995).

[22]T. Diaz de la Rubia, A. Caro, and M. Spaczer, Phys. Rev. B 47, 11 483 (1993).

[23]A. Y. Stathopoulos, C. A. English, B. L. Eyre, and P. B. Hirsch, Philos. Mag. A 44, 309 (1981).

[24]M. Ghaly and R. S. Averback, Phys. Rev. Lett. 72, 364 (1994).

[25]R. S. Averback and M. Ghaly, Nucl. Instrum. Methods B 90, 191 (1994).

[26]M. Spaczer, A. Caro, M. Victoria, and T. Diaz de la Rubia, Phys. Rev. B 50, 13 195 (1994); Proceedings of COSIRES '94, Santa Barbara, 1994 [Rad. Effects Def. Sol (to be published)].

[27]A. F. Calder, Ph.D. thesis, Liverpool University, 1990.